

"Crater" flux transfer events: Highroad to the X line?

C.J J Farrugia, Li-Jen Chen, R.B. Torbert, D.J. Southwood, S.W.H. Cowley, A Vrublevskis, C Mouikis, A Vaivads, M André, Pierrette Décréau, et al.

▶ **To cite this version:**

C.J J Farrugia, Li-Jen Chen, R.B. Torbert, D.J. Southwood, S.W.H. Cowley, et al.. "Crater" flux transfer events: Highroad to the X line?. Journal of Geophysical Research Space Physics, 2011, 116 (A2), pp.A02204. 10.1029/2010JA015495 . insu-01371563

HAL Id: insu-01371563
https://insu.hal.science/insu-01371563

Submitted on 5 Dec 2016

HAL is a multi-disciplinary open access archive for the deposit and dissemination of scientific research documents, whether they are published or not. The documents may come from teaching and research institutions in France or abroad, or from public or private research centers.

L'archive ouverte pluridisciplinaire **HAL**, est destinée au dépôt et à la diffusion de documents scientifiques de niveau recherche, publiés ou non, émanant des établissements d'enseignement et de recherche français ou étrangers, des laboratoires publics ou privés.

"Crater" flux transfer events: Highroad to the X line?

C. J. Farrugia,[1] Li-Jen Chen,[1] R. B. Torbert,[1] D. J. Southwood,[2] S. W. H. Cowley,[3] A. Vrublevskis,[4] C. Mouikis,[1] A. Vaivads,[5] M. André,[5] P. Décréau,[6] H. Vaith,[1] C. J. Owen,[7] D. J. Sibeck,[8] E. Lucek,[9] and C. W. Smith[1]

Received 22 March 2010; revised 24 September 2010; accepted 1 December 2010; published 8 February 2011.

[1] We examine Cluster observations of a so-called magnetosphere "crater FTE," employing data from five instruments (FGM, CIS, EDI, EFW, and WHISPER), some at the highest resolution. The aim of doing this is to deepen our understanding of the reconnection nature of these events by applying recent advances in the theory of collisionless reconnection and in detailed observational work. Our data support the hypothesis of a stratified structure with regions which we show to be spatial structures. We support the bulge-like topology of the core region (R3) made up of plasma jetting transverse to reconnected field lines. We document encounters with a magnetic separatrix as a thin layer embedded in the region (R2) just outside the bulge, where the speed of the protons flowing approximately parallel to the field maximizes: (1) short (fraction of a sec) bursts of enhanced electric field strengths (up to ~30 mV/m) and (2) electrons flowing against the field toward the X line at approximately the same time as the bursts of intense electric fields. R2 also contains a density decrease concomitant with an enhanced magnetic field strength. At its interface with the core region, R3, electric field activity ceases abruptly. The accelerated plasma flow profile has a catenary shape consisting of beams parallel to the field in R2 close to the R2/R3 boundary and slower jets moving across the magnetic field within the bulge region. We detail commonalities our observations of crater FTEs have with reconnection structures in other scenarios. We suggest that in view of these properties and their frequency of occurrence, crater FTEs are ideal places to study processes at the separatrices, key regions in magnetic reconnection. This is a good preparation for the MMS mission.

Citation: Farrugia, C. J., et al. (2011), "Crater" flux transfer events: Highroad to the X line?, *J. Geophys. Res.*, *116*, A02204, doi:10.1029/2010JA015495.

1. Introduction

[2] In a major breakthrough in space research, *Russell and Elphic* [1978] discovered flux transfer events (FTEs), which they interpreted as signatures of reconnection between the magnetosphere and magnetosheath magnetic field lines taking place in a bursty fashion. FTEs have since formed a centerpiece of studies of reconnection at the dayside magnetopause. FTEs were identified in magnetic field data during crossings of the low-latitude magnetopause by the ISEE-1/-2 spacecraft. Signatures called "flux erosion events" were seen even earlier in the data returned by the HEOS-2 probe at high latitudes [*Haerendel et al.*, 1978], which were shown to be equivalent to FTEs [*Rijnbeek and Cowley*, 1982]. The basic FTE signature consists of a bipolar variation of the field component normal to the magnetopause (B_n), which is often accompanied by simultaneous deflections in the tangential components. They are typically of ~1 min duration with a peak-to-peak excursion of B_n ~ 10 nT. In interpreting these signatures in terms of reconnection, Russell and Elphic proposed a cartoon in which two bundles of reconnected field lines form two elbow-shaped, isolated flux tubes of open field lines which propagate away from the reconnection site in the northward and southward directions, respectively. This conceptual model, which is based on reconnection at an X line of limited spatial extent, influenced studies of transient reconnection and its ionospheric imprints for many years. The underlying reconnection interpretation of FTEs was

[1]Space Science Center, Department of Physics, University of New Hampshire, Durham, New Hampshire, USA.
[2]ESA Headquarters, Paris, France.
[3]Department of Physics and Astronomy, University of Leicester, Leicester, UK.
[4]Plasma Science and Fusion Center, Massachusetts Institute of Technology, Cambridge, Massachusetts, USA.
[5]Swedish Institute of Space Physics, Uppsala, Sweden.
[6]LPCE2/CNRS, Orleans, France.
[7]Mullard Space Science Laboratory, University College London, London, UK.
[8]NASA Goddard Space Flight Center, Greenbelt, Maryland, USA.
[9]Space and Atmospheric Physics Group, Imperial College of Science and Technology, London, UK.

Copyright 2011 by the American Geophysical Union.
0148-0227/11/2010JA015495

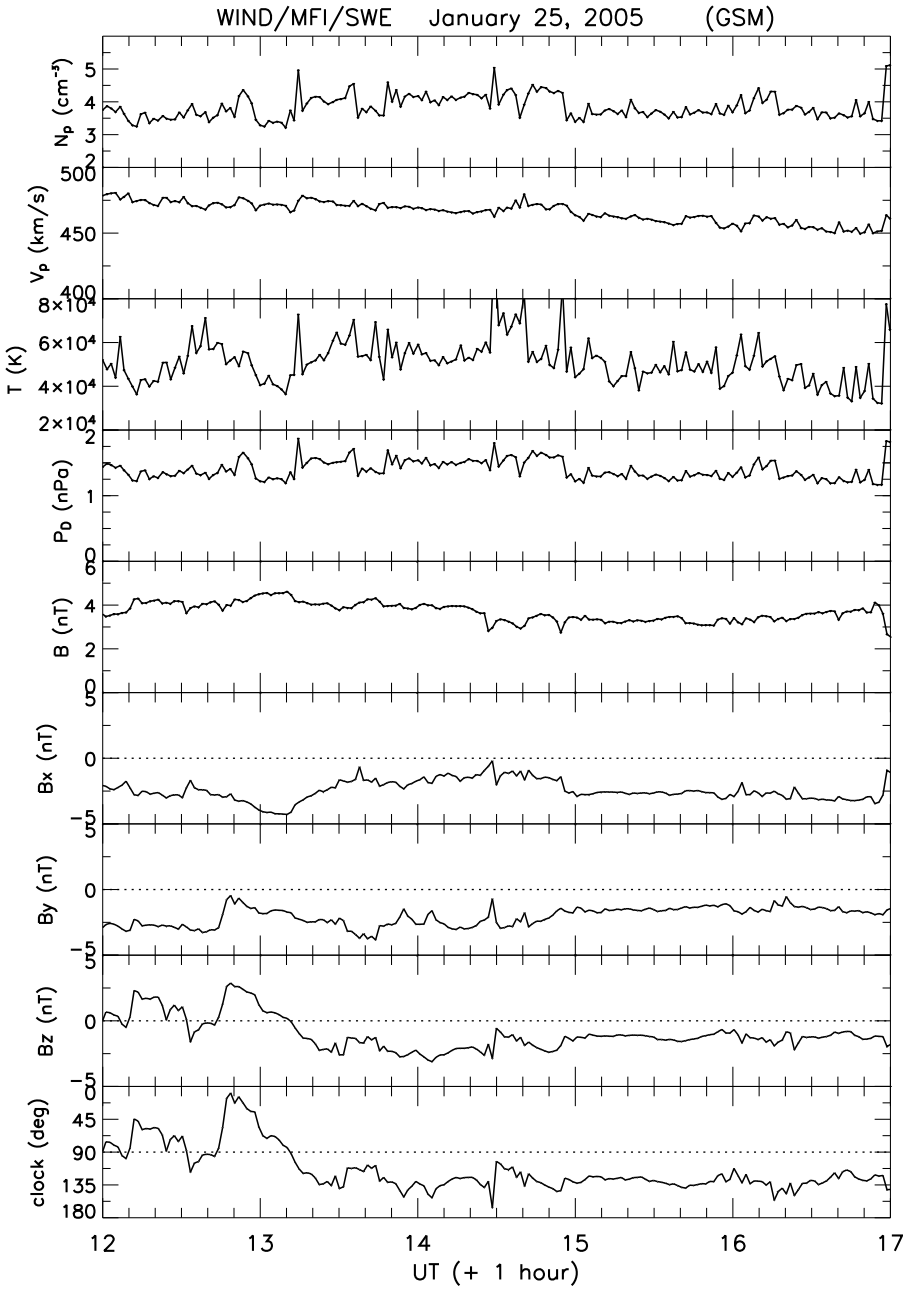


Figure 1. Interplanetary plasma and magnetic field data from the SWE and MFI instruments on Wind for the interval 12–17 UT, 25 January 2005. From top to bottom plots show the proton density, bulk speed, temperature, dynamic pressure, the total magnetic field strength and its GSM components, and the IMF clock angle. The UT has been shifted by 1 h to take account for the estimated convection delay time it takes for the signals to reach the subsolar magnetopause.

subsequently supported by plasma [e.g., *Paschmann et al.*, 1982; *Southwood et al.*, 1988] and energetic particle data [*Scholer et al.*, 1982; *Daly et al.*, 1981; *Daly and Keppler*, 1983] and has remained the standard explanation.

[3] An elaboration of the flux rope model of FTEs was put forward by *Cowley* [1982] and *Paschmann et al.* [1982], independently, and confirmed experimentally by *Saunders et al.* [1984]. This concerns the continuity of the B_n signature and the occasional presence of deflections in the orientation of the flux tube field away from the direction of the field on the opposite side of the magnetopause (so called "away" tilts [*Cowley*, 1982]). Part of this signature arises from draping when the field and flow lines are displaced by the moving obstacle. (This process was investigated in the incompressible flow limit by *Southwood* [1985] and *Farrugia et al.* [1987] and employed to remote sense FTEs [e.g., *Papamastorakis et al.*, 1989; *Walthour et al.*, 1993] and plasmoids in the geomagnetic tail [*Slavin et al.*, 1989; *Moldwin and Hughes*, 1991].) The suggestion that the magnetic field spirals around the axis of the flux tube

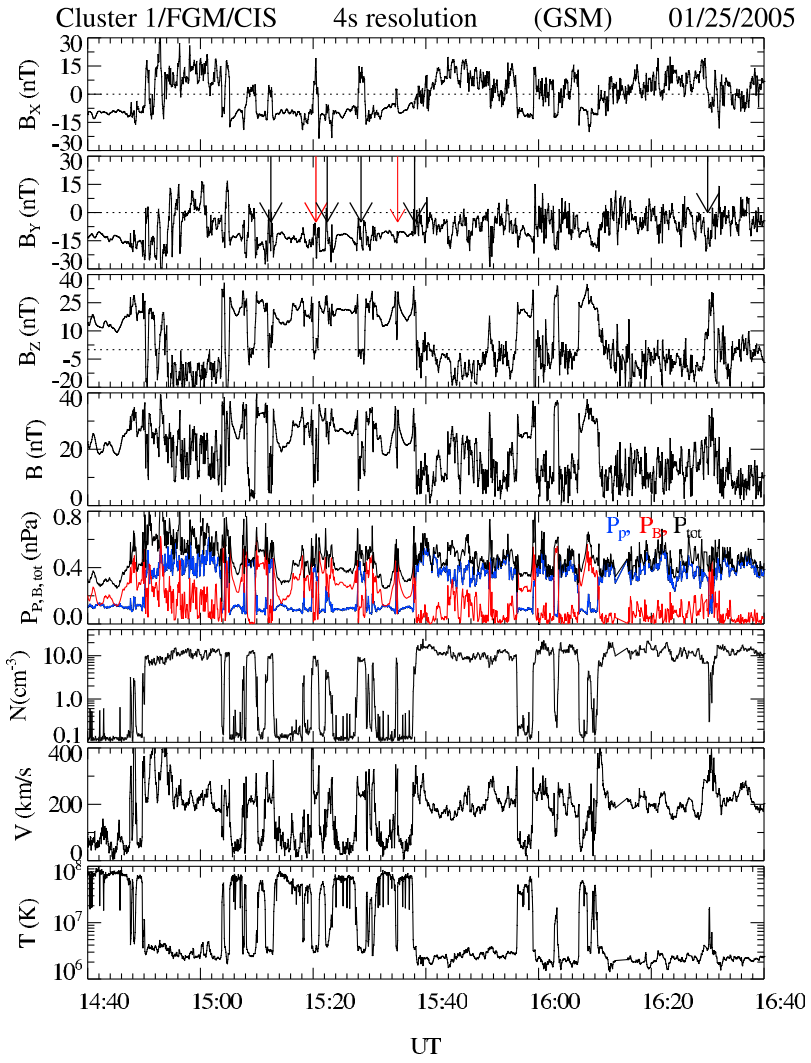


Figure 2. Cluster 1 magnetic field and plasma data from the FGM and CIS/HIA instruments for period 1440–1640 UT. From top to bottom plots show the GSM components of the magnetic field and the total field strength, the pressures (plasma in blue, magnetic in red, and total in black), the density, bulk speed, and temperature.

[*Cowley*, 1982; *Paschmann et al.*, 1982] was explained theoretically by *Sonnerup* [1987]. Twisted field lines have the further pleasing feature of being able to explain the evident stability of these structures where there is often a total (field + plasma) pressure excess: namely, the inward-pointing pinch force ($\mathbf{B} \cdot \nabla \mathbf{B}$) on the core balances the outward-pointing pressure (field + plasma) gradient force ($-\nabla P$) [*Paschmann et al.*, 1982; *Southwood et al.*, 1988]. Clearly, twisted internal field lines imply a distributed current flowing along the "axis" of the tube with possibly a return current along the flanks. Corresponding predictions on flow and magnetic disturbances at the ionospheric footprint of FTEs were made [*Saunders et al.*, 1984; *Southwood*, 1987; *McHenry and Clauer*, 1987], all based on the notion of an isolated flux tube propagating northward/southward.

[4] A departure from the basic idea of an isolated flux tube was that of *Rijnbeek et al.* [1987]. They examined AMPTE/UKS data at higher resolution (two samples/s for **B**) for a magnetospheric FTE on 28 October 1984. They could identify both the draping as well as the open field line regions in the magnetic field and plasma data. In addition, however, they detailed some properties of a third regime nested between these two. (They called these regions R1, R2, R3, which are crossed in reverse order as the spacecraft exits the structure.) A major feature characterizing the new region R2 is a deflection of magnetic field in the *LM* plane (the local magnetopause surface) in the opposite sense to its rotation in the draping (R1) and core (R3) regions of the FTE, implying a separate current flowing near the boundary of the structure. Inside R2, Rijnbeek et al. showed indications of energization in the electron and ion populations, and thus suggested that R2 might contain newly opened lines, i.e., field lines being opened even as the observations are being made. This is in contrast with the field lines in R3, which were opened some time in the past. The idea of continued reconnection was proposed also by *Scudder*

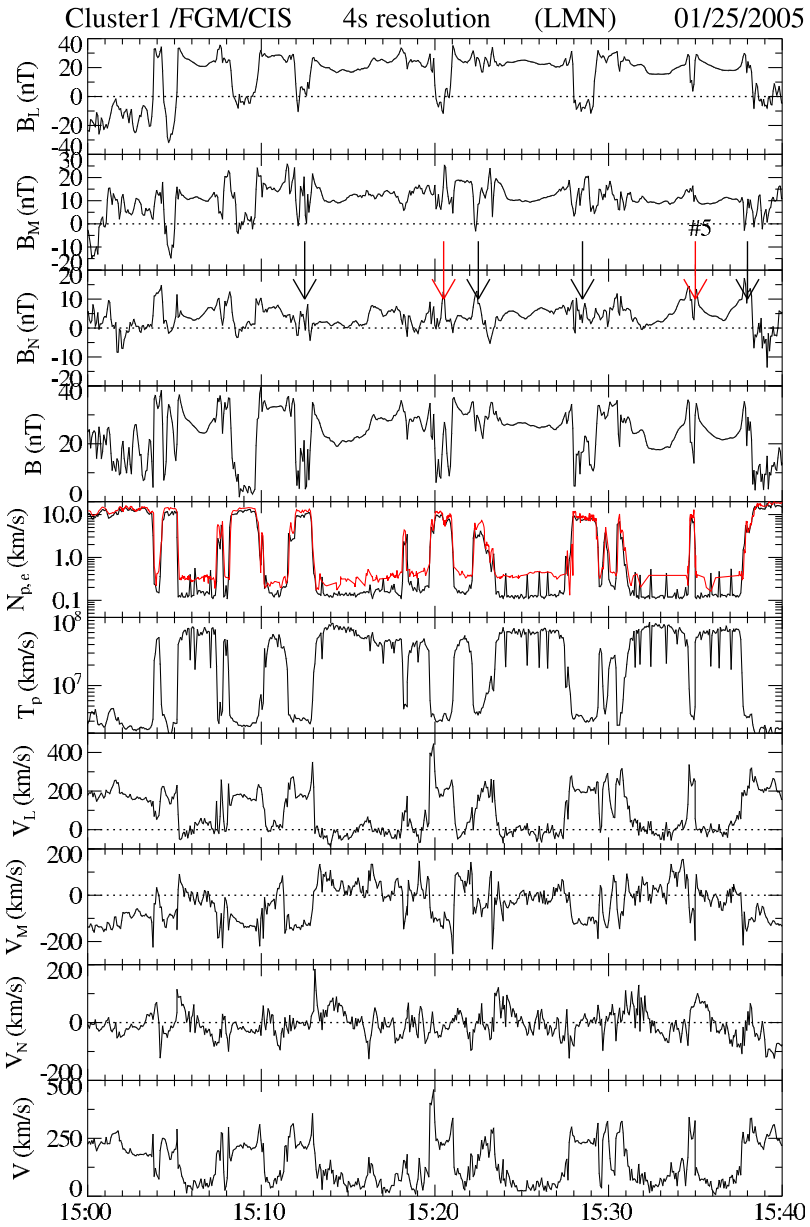


Figure 3. Cluster 1 magnetic field and plasma observations in boundary normal coordinates (*LMN*) for the interval 1500–1540 UT. The FTEs (arrowed) are all magnetospheric FTEs because the spacecraft starts and ends in the magnetosphere/boundary layer. The duration of each is ~1–2 min.

et al. [1984], who noted heat flux layers composed of electrons streaming along the boundary. Clearly, the observations called for a modification of the isolated flux tube model because they implied a different topology, namely, one where some outer field lines are still connected to the reconnection X line (see the review by *Farrugia et al.* [1988]).

[5] Extending *Rijnbeek et al.*'s [1987] work to other events, *Farrugia et al.* [1988] noted a multilayered structure in the plasma and magnetic field of magnetospheric FTEs, i.e., those where the spacecraft starts and ends in the magnetosphere. They examined data from four instruments on AMPTE/UKS. Consistent with the observation of *LaBelle et al.* [1987], they noted the peculiar temporal profile of the field strength which does not simply rise to a maximum and decrease. Rather, it has a "W" or "M"-shaped variation, with a maximum bracketed by two minima or vice versa. Sometimes it was even more complicated than that. This profile prompted *LaBelle et al.* [1987] to term this class of FTEs, "crater FTEs," and the extreme dips in the field were reminiscent of magnetopause magnetic holes [see *Lühr and Klöcker*, 1987]. Flow shears (to the magnetic field) were a common feature of the observations, including in two cases a reversal of the flow in R3 (counter-streaming flows in R3) [see *Farrugia et al.*, 1988, Figure 10]. Further, it was suggested that the core region was indistinguishable from the surrounding magnetosheath. Different wave activities were shown to characterize the various regions of the FTE by

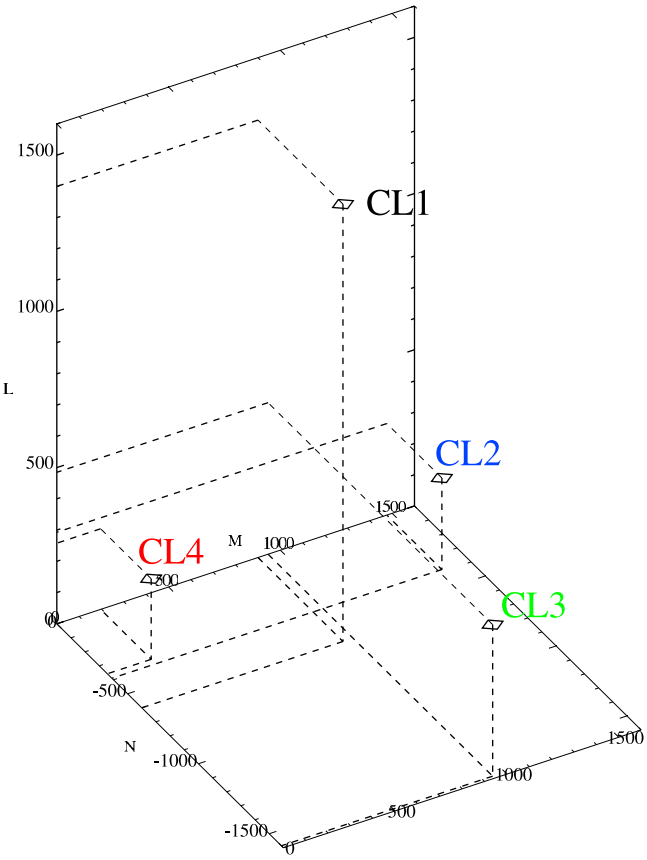


Figure 4. The relative positions of the spacecraft during their observations of the FTE we study. The view is from the magnetosphere. The *LM* plane (vertical) is the notional magnetopause. Figure 4 is constructed by first assigning an arbitrary normal distance of C1 from the magnetopause (600 km).

LaBelle et al. [1987]. In summary, Farrugia et al.'s work, too, implied that a more elaborate model than the isolated flux tube was needed to do full justice to the observations.

[6] The task of formulating such a model was undertaken by *Southwood et al.* [1988] and *Scholer* [1988], independently. The model, while qualitative, was intrinsically three-dimensional. Southwood et al. proposed a bubble of reconnected, twisted fields and plasma being created on the magnetopause by a surge in the reconnection rate. The passage of this bubble over a spacecraft as it is propelled away from the elongated X line by magnetic tension forces gives rise to the complex FTE signature. In the absence of collisions, the outflow consists initially of field-aligned beams, which are then heated. The resulting plasma pressure inflates the structure so that it acquires a bubble cross section. Beams of particles are flowing on its outskirts when these are still connected to the X line. The flow shear across the boundary results in a skewing of the magnetic field across the boundary, giving rise in this way to the internal twisted field. There was nothing in the model to determine the scale size perpendicular to the direction of motion of the bulge along the magnetopause so that, in principle, this could be very large, with obvious repercussions on the ionospheric imprint of crater FTEs. Basic differences from the Russell and Elphic picture emerged from this theoretical framework. The work of *Southwood et al.* [1988] [see also *Scholer*, 1988] made a juncture with theoretical work predicated upon changes in the reconnection rate in a Petschek-type scenario [*Biernat et al.*, 1987], but was not restricted to the limit of small perturbations as in the latter work.

[7] Clearly, these advances in the 1980's were made possible in part by the higher resolution of the magnetic field data and through the use of a complement of instruments. Yet, without multispacecraft observations and even higher time resolution, the reason behind the stratification of fields and plasmas in crater FTEs, and the detailed structure of the R2 region, remained something of an enigma, not least the flow shears [*Farrugia et al.*, 1988; *Southwood et al.*, 1988]. Thus that R2 contains a separatrix as a fine structure within it was not conclusively established observationally. It is the purpose of this paper to analyze the structure of a crater FTE further, using the multi-instrument, multispacecraft capability of Cluster. It was one of a sequence observed in the magnetosphere during an outbound pass on 25 January 2005. We shall discuss measurements made by the Fluxgate Magnetometer (FGM) [*Balogh et al.*, 1997], Cluster Ion Spectrometry experiment (CIS) [*Rème et al.*, 1997], Electron Drift Instrument (EDI) [*Paschmann et al.*, 1997], the Plasma Electron and Current Experiment (PEACE) [*Johnstone et al.*, 1995], the Electric Field and Wave Experiment [*Gustafsson et al.*, 1997], and the Waves of High frequency and Sounder for Probing Electron density by Relaxation experiment (WHISPER) [*Décréau et al.*, 2001]. We shall also bring to bear very high resolution (67 samples/s) magnetic field data from FGM, electron data from EDI at 128 samples/s when working in ambient mode, and EFW data in burst mode at a sampling rate of 450 Hz.

[8] Our approach is to order the data within the conceptual framework of the papers discussed above, seeking to find the various layers and other physical properties characterizing them. We shall then extend the reconnection interpretation of the observations using newer insights gained on collisionless reconnection from numerical simulations and detailed data analysis on the microphysics of the reconnection process. We shall focus on the structure of R2 and show that there is a thin layer embedded in it which is characterized by various signatures of a magnetic separatrix, i.e., a surface made up of magnetic field lines still connected to the X line. Various indicators suggest this lies close to the R2/R3 interface. Finally, we shall also mention some features that crater FTEs have in common with observations of reconnection in contexts other than the magnetopause.

2. Interplanetary Observations: Wind

[9] Figure 1 shows interplanetary plasma and magnetic field data from the Solar Wind Experiment (SWE) [*Ogilvie et al.*, 1995] and Magnetic Field Investigation (MFI) [*Lepping et al.*, 1995] on spacecraft Wind for the interval 12–17 UT, 25 January 2005. From top to bottom, the panels display the proton density, bulk speed, and temperature, the dynamic pressure, the total magnetic field strength and its components in GSM coordinates, and the IMF clock angle,

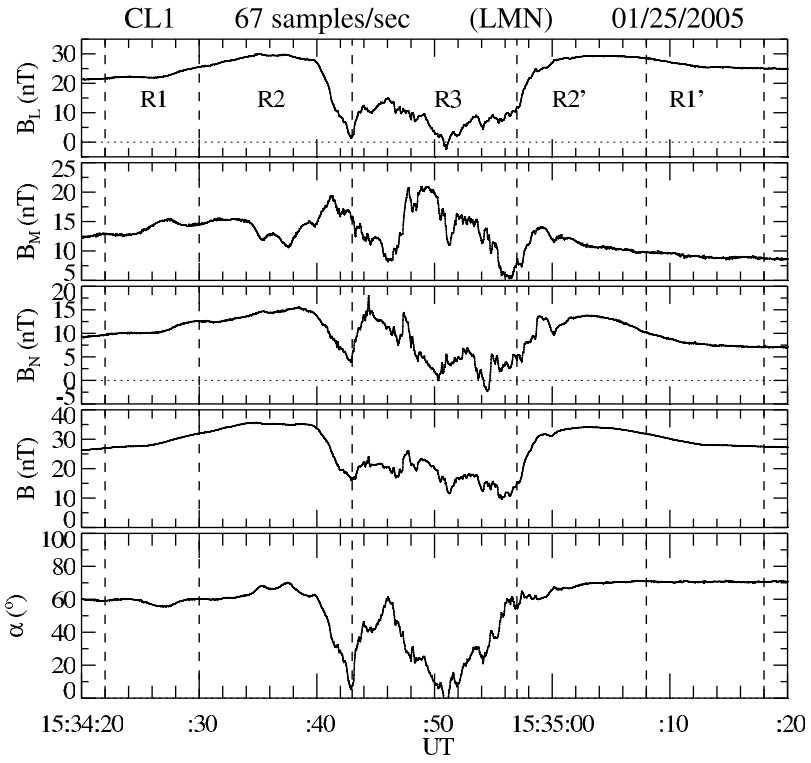


Figure 5. Cluster 1 magnetic field data in LMN coordinates plotted at a temporal resolution of 67 samples/s. The bottom plot shows the angle α, defined as the angle subtended by the field in the (LM) plane (i.e., magnetopause) to the M axis, increasing toward the $+L$ direction (northward). Region designations R1-R2-R3-R2′-R1′ have been marked. For further details, see text.

i.e., the polar angle in the GSM YZ plane. Wind was in orbit around the L1 Lagrangian point and at the center of the interval it was located at (255, −27, 18) R_E (Earth radii; GSE coordinates). From ~13 UT, Wind observes a southwesterly IMF (clock angle ≈ 130°) in a marginally fast solar wind stream of fairly steady dynamic pressure. The negative B_z is conducive to magnetopause reconnection. With an average speed of ~460 km s^{-1}, the convective delay to the subsolar magnetopause is ~1 hr. This time delay has been added to the abscissa. A more exact delay is not needed since the interplanetary conditions are steady during the time when the magnetopause observations considered below were made.

3. Magnetopause Observations: Overview From Cluster 1

[10] At ~15 UT in 25 January 2005, Cluster was outbound at postnoon magnetic local times (MLT ~ 15 hr) and magnetic latitudes (MLAT) of ~28.3°. The spacecraft separation is of order 1200 km. Figures 2 and 3 give an overview of magnetic field and plasma (proton and electron) observations from data acquired by Cluster 1 (C1). Figure 2 presents the magnetic field and plasma measurements from the FGM and CIS/HIA instruments for the 2 h interval 1440–1640 UT. The panels show the components of the magnetic field in GSM coordinates and the total field strength. Then follow the pressure (plasma in blue, magnetic in red, and total in black), the density, bulk speed and temperature. The spacecraft starts in the magnetosphere, crosses into the magnetosheath at ~1450 UT, makes a long encounter with the boundary layer from 1508–1538 UT, after which it is mainly in the magnetosheath. The boundary layer period is the interval of interest here.

[11] In the magnetosheath the plasma pressure consistently dominates the magnetic pressure (plasma $\beta > 1$), and the reverse is the case in the magnetopause/boundary layer. Marked by arrows in the second panel are some FTEs, all of the crater variety. The first six are magnetospheric, while the last one at ~1630 UT is a magnetosheath FTE. During the encounters with the FTEs there is a strict antiphase correlation between the plasma and magnetic pressures. In the FTEs the total pressure (fifth panel) is above ambient with the plasma and magnetic pressures alternating in providing this excess. Contrast this with the boundary layer between the FTEs (where $P_B > P_P$ consistently) and the magnetosheath (where $P_P > P_B$ consistently).

[12] We next rotate coordinates from GSM to Boundary Normal [*Russell and Elphic*, 1978]. To do this, we obtain the magnetopause normal $\hat{\mathbf{N}}$ by forming a cross product between the magnetosphere and magnetosheath field, taking averages over 1440–1446 UT for the former and from 1452–1500 UT for the latter. Using $\hat{\mathbf{N}}$, we form a right-handed triad (LMN). Unit vectors in the L- and M- directions are tangential to the local magnetopause surface in such a way that the LN plane contains the GSM z axis. Finally, we obtain the unit vectors in GSM coordinates $\hat{\mathbf{L}}$ =

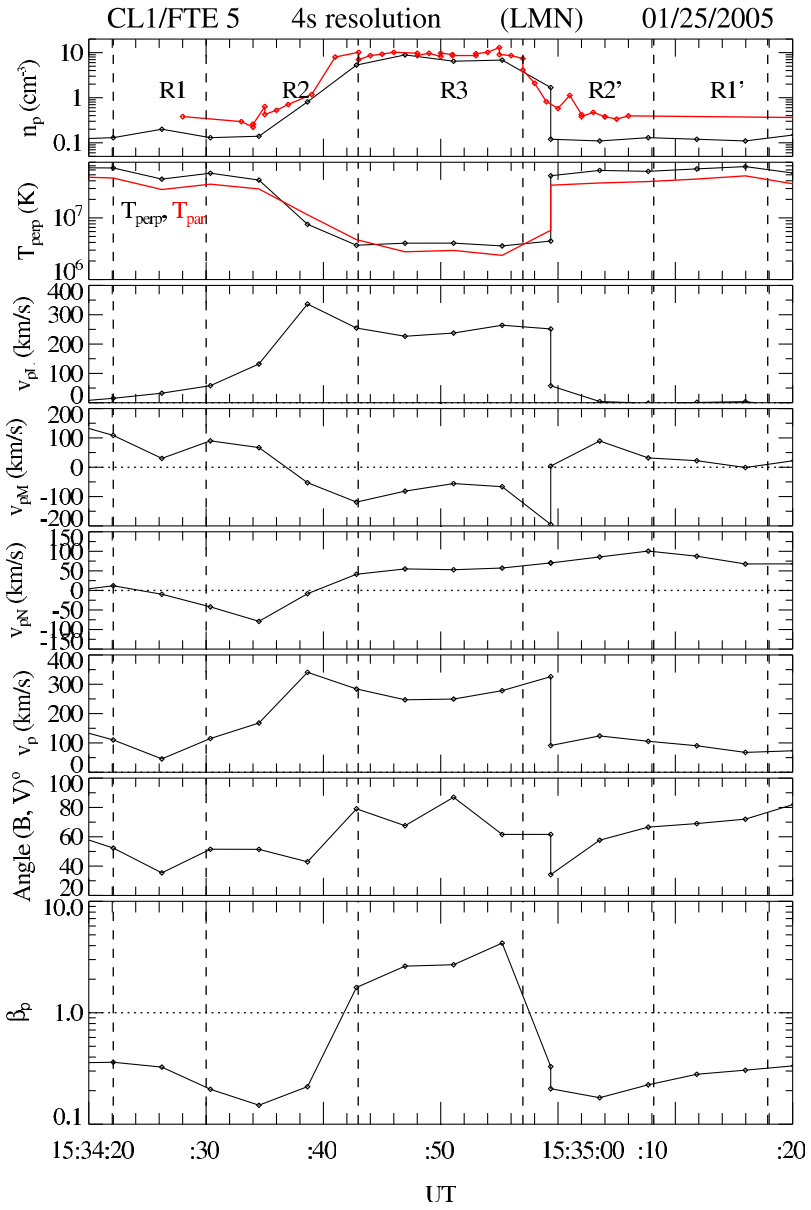


Figure 6. Cluster 1/CIS/HIA plasma data for the interval 1534:20–1535:20 UT. From top to bottom the plots show the density (density inferred from the WHISPER instrument shown in red), temperatures, velocity components (LMN coordinates) and total bulk speed, the angle between the field and the flow vectors, and the proton β.

(−0.65, −0.09, 0.75) (i.e., pointing mainly north), $\hat{\mathbf{M}}$ = (0.14, −0.99, 0.0) (mainly west) and $\hat{\mathbf{N}}$ = (0.75, 0.10, 0.66).

[13] Figure 3 shows C1 magnetic field and plasma observations in *LMN* coordinates for the shorter interval 1500–1540 UT, encompassing the boundary layer traversal (1504–1538 UT). The FTEs are arrowed. They are all magnetospheric FTEs because the spacecraft starts and ends in the magnetosphere/boundary layer. The duration of each is ~1–2 min. Evident is the general bipolar variation in the field component normal to the magnetosphere, a defining characteristic of FTEs. The temporal profile of the total field strength contains two or more relative minima, typical of crater FTEs. It is generally lower than the surrounding field in the boundary layer. The fifth panel shows the proton (black trace) and electron densities (red trace) from CIS/HIA and WHISPER, respectively, both at 4 s temporal resolution. The electron density is obtained from the plasma frequency by the relation $N_e = f_{pe}^2/80.64$ with f_{pe} in kHz. Values of N_e when f_{pe} is less than 10 kHz (i.e., values below ~1 cm^{-3}) are considered indicative rather than definitive. The difference between CIS/ion and WHISPER/electron densities indicates that there are cold ions present (few eV, low as compared with the spacecraft potential.) The electron and proton densities tend to increase in each FTE. The flow speeds (Figure 3, bottom) tend to maximize at the edges of the events and they can be very high there,

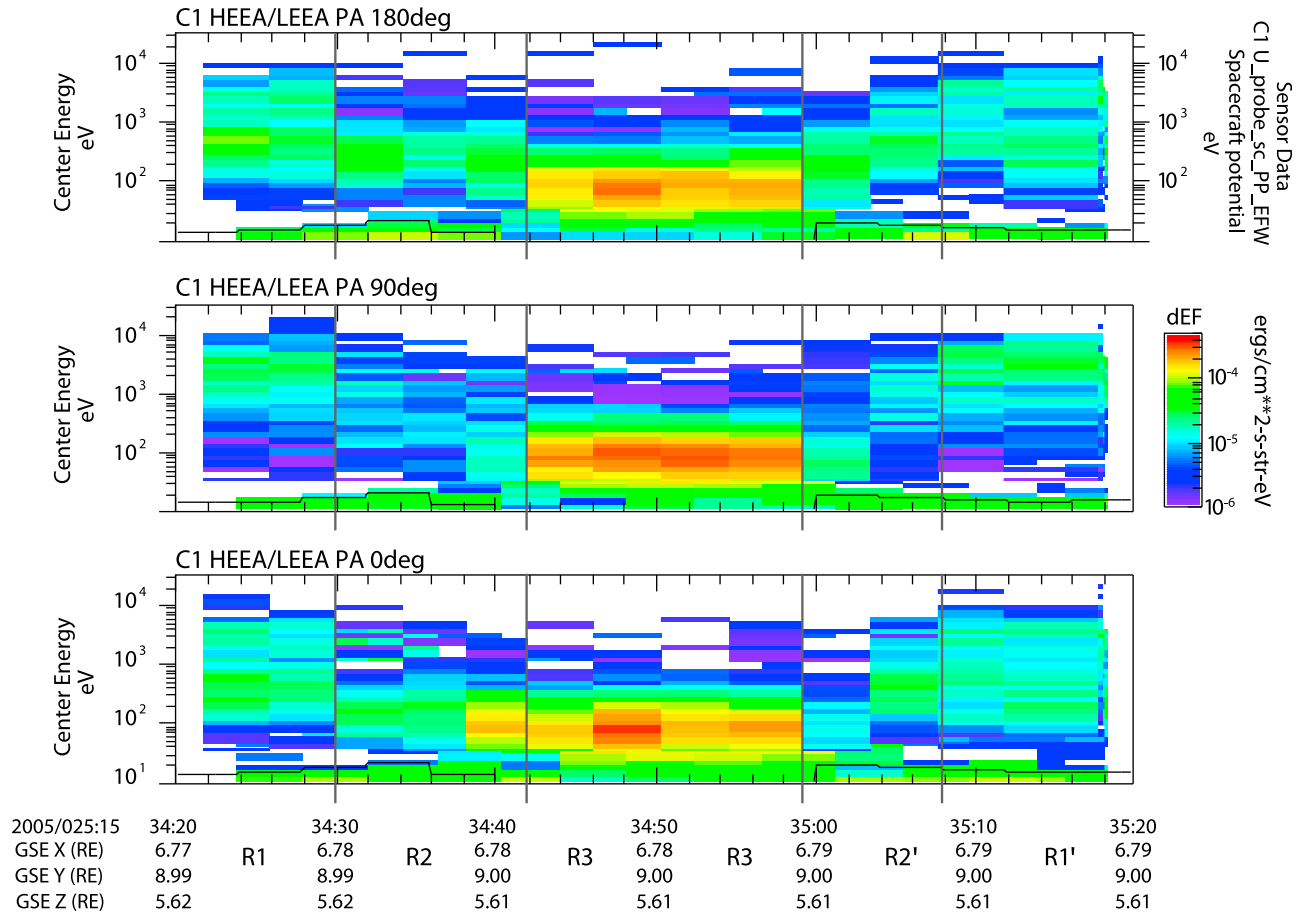


Figure 7. Cluster 1 electron differential energy fluxes from the PEACE instrument for the interval 1534:20–1535:20 UT plotted as a function of time and energy. The pitch angles are displayed: (top) 180°, (middle) 90°, and (bottom) 0°.

exceeding in many cases the average speed of the magnetosheath plasma.

4. Flux Transfer Event: 1534:20–1535:20 UT

4.1. Cluster 1 Observations

[14] We now direct attention to FTE 5, giving first observations made by C1 and then summary observations made by all four spacecraft.

[15] Figure 4 shows the relative positions of the spacecraft during their observations of the FTE. The view is from the magnetosphere. The *LM* plane (vertical) is the notional magnetopause. The magnetopause normal was used to express the relative positions of the spacecraft along the L, M, N axes. We arbitrarily set the normal distance of C1 from the magnetopause to be 600 km so that all the spacecraft fit in nicely. Figure 4 therefore correctly gives the relative positions of the spacecraft, but the absolute distances from the magnetopause are arbitrary.

[16] The C3 spacecraft is the one most displaced in the $-\hat{\mathbf{N}}$ direction. C2 and C4 have comparable separations along N and are separated mainly (by ~1300 km) along M (east-west). C1 has the largest displacement along L, lying north of the other spacecraft. In many ways this is an ideal spacecraft configuration to test whether a bulge of reconnected field and plasma is sweeping past along the magnetopause since the duration of its passage would be different at the various spacecraft. It is also an ideal configuration to test the presence of, and fine structures in, the various layers in and around this bulge, assuming they are spatial: some spacecraft may miss a layer, and a substructure may only be encountered briefly. However, the spacecraft configuration is not very suitable to infer anything but a rough lower limit on its extent of the bulge in the east-west (*M*) direction, and heights above the magnetopause are somewhat uncertain.

[17] We now focus on observations of the FTE made by C1. Figure 5 shows the magnetic field data in boundary normal coordinates at a temporal resolution of 67 samples/s for the 1 min interval 1534:20–1535:20 UT: The *L*, *M*, *N* components, the total field, and the angle α, defined as the angle subtended by the field in the (LM) plane (i.e., magnetopause) to the *M* axis, increasing toward the +*L* direction (northward). Region designations R1-R2-R3-R2′-R1′ have been marked. These were arrived at by a study of the magnetic field data from FGM and proton data from CIS (except for C2, where we use instead electron data from the PEACE instrument), as described below.

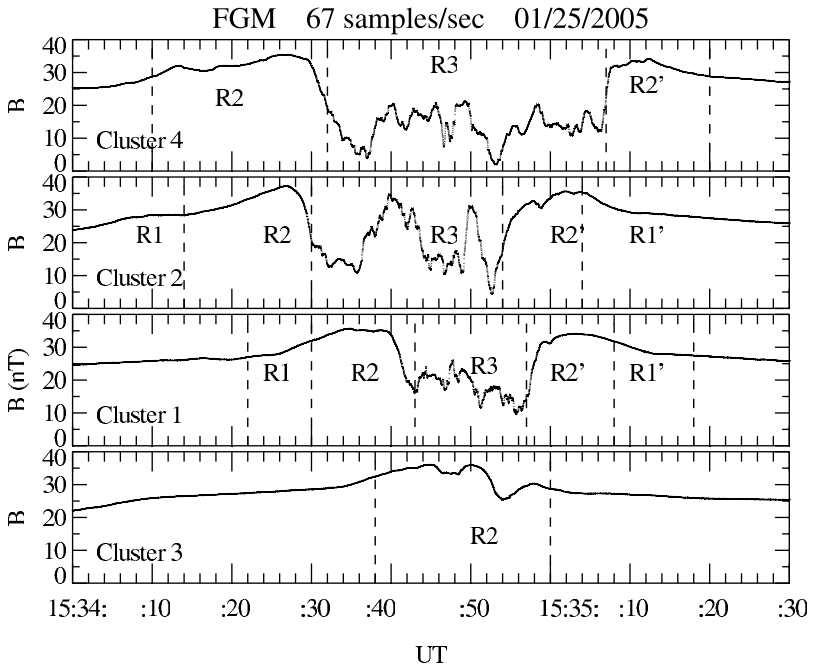


Figure 8. The magnetic field strength profiles, plotted from top to bottom in order of increasing distance from the magnetopause. The duration of the signature varies inversely with normal distance to the magnetopause.

[18] The following features are worth noting. (1) In R2 the magnetic field deviates from its orientation and strength in the draping region R1. In particular, it executes a large rotation, turning first northward and then deflects sharply westward, so that it points almost due west at the R2/R3 interface. This is indicative of a current at the R2/R3 boundary. It is also much enhanced in strength in the central part of the region. Compared to R3, the field in R2 is relatively smooth. Qualitatively similar features occur in R2′. (2) The field profile in R3 has a complicated shape with several local maxima and minima. The minima can sometimes be very deep approaching magnetic nulls, for example on C4 (the spacecraft closest to the magnetopause; see Figure 8 below). The general field strength is lower than in the surrounding regions. (3) In R3 there are also high-frequency small-amplitude variations in all field components, including B_N. However, an average sinusoidal variation in the latter component can still be distinguished, though there is an offset. (3) Regions are traversed in reverse order as the spacecraft moves out of the structure. A nesting and layering is generally evident in these data.

[19] For the same interval, Figure 6 shows CIS/HIA plasma data at 4s spin resolution: the density (in red: density inferred from the WHISPER instrument), the temperatures, the velocity vector in *LMN* coordinates and total bulk speed, the angle between the field and the flow vectors, and the proton plasma beta. Here region R2 is identified by the gradients in N and T. In R2 the density shows a small decrease to values lower than in R3 and R1. (A similar feature occurs on other spacecraft, also in R2, where there is data, see Figure 15 below.) This is a density depletion which will be discussed further in connection with Figure 15. The velocity vector shows pronounced shears with the magnetic field vector. The bulk speed profile exhibits maxima ("horns") in R2, where the angle of the flow with the field (seventh panel) is smaller than in R3. This high-speed burst occurs close (i.e., within 1 data points) to the interface of R2 with R3. The flow in R3 is mainly along +L and −M (i.e., northward and eastward). Interpreting this as the effect of a slingshot action exerted by the magnetic field, we infer an X line location which is south and west of the spacecraft, an inference which is also consistent with the average B_N profile. The proton plasma β_p, which as we saw is a good tracer of the various regions, is $\gg 1$ in R3, where the plasma thus dominates the magnetic field, but reaches a minimum of ≈ 0.15 in R2, where the influence of the magnetic field is dominant.

[20] Figure 7 shows electron spectrograms from PEACE for the same 1 min interval as in Figures 5 and 6. The (color coded) differential energy fluxes are plotted as a function of time and energy. Region R3, as defined from CIS and FGM, embraces the region of intense low-energy fluxes (around 100 eV, typical of the magnetosheath). Region R2 has strong flows along antiparallel (Figure 7, top) and parallel (Figure 7, bottom) to the field over the approximate energy range 40–700 eV.

4.2. Summary Plots From Multiple Spacecraft: Separatrix Within R2

[21] We now study various properties of the FTE using summary plots of key physical quantities from multiple spacecraft. In particular, one aim is to show that R2 contains a substructure which may be identified as a magnetic separatrix, i.e., a surface consisting of all field lines passing through the reconnection X line. We shall discuss (1) the profiles across the FTE of the magnetic

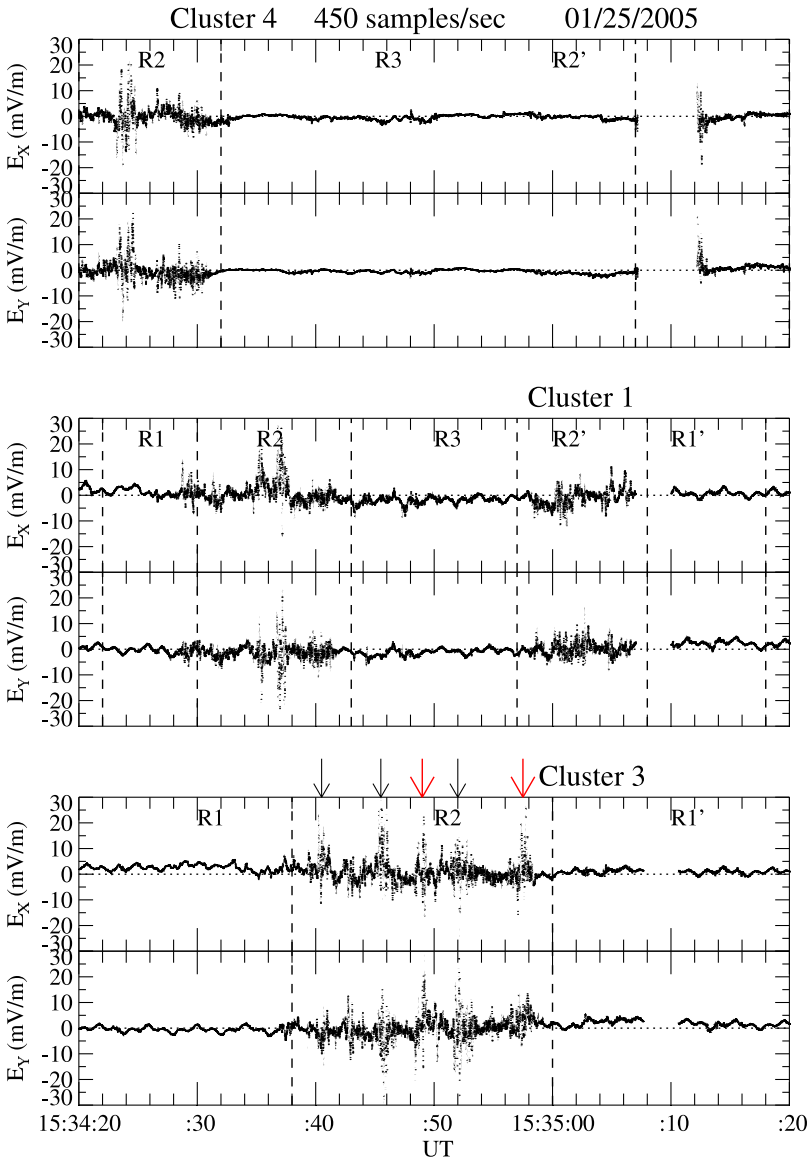


Figure 9. Electric field measurements from the EFW instrument showing two spin-plane component (X, Y ~GSE) measurements from the double probe instrument on C4, C1, and C3. The temporal resolution is 450 Hz. The region boundaries are set by the FGM and CIS data, as described in the text. Arrowed in the bottom plot are the discrete bursts of enhanced electric field activity.

field strength, (2) electric field activity, (3) electron distribution functions, (4) electron flows in region R2 from the EDI instrument, (5) the accelerated plasma flow profiles, (6) the ion distribution functions in R2, and (7) the density profiles. The region designations and their extents were arrived at by a similar procedure as that for C1, i.e., with the joint use of FGM and CIS data. These region boundaries are then incorporated in the plots of other quantities (e.g., **E** fields, EDI and PEACE electrons), so that a relevant question is whether these boundaries still order the data of these other quantities well. Importantly, a major emphasis is on the structure of R2, where we shall show various signatures (in electron and ion flows, electric field turbulence and plasma density) of encounters with a magnetic separatrix embedded in this region.

4.2.1. Magnetic Field Strength Profiles

[22] Figure 8 shows the *B* field profiles. They are plotted from top to bottom in order of increasing distance from the magnetopause (see Figure 4). The distances from the model magnetopause are C4, 360 km; C2, 390 km; C1, 600 km; C3, 1590 km. Clearly, the spacecraft see nested signatures, the duration of the inner region R3 decreasing as the spacecraft distance from the magnetopause increases. Thus C4, C2 and C1 see apparently similar, nested signatures, that on C2/C1 being scaled down version of that on C4. C2 and C4 enter the structure approximately simultaneously. C3 misses region R3 altogether (see further below).

[23] In R3, C4, C2, and C1 see instances of very low magnetic field strengths, approaching one occasion (C4 at 1534:53 UT) magnetic nulls. These field minima in R3 are

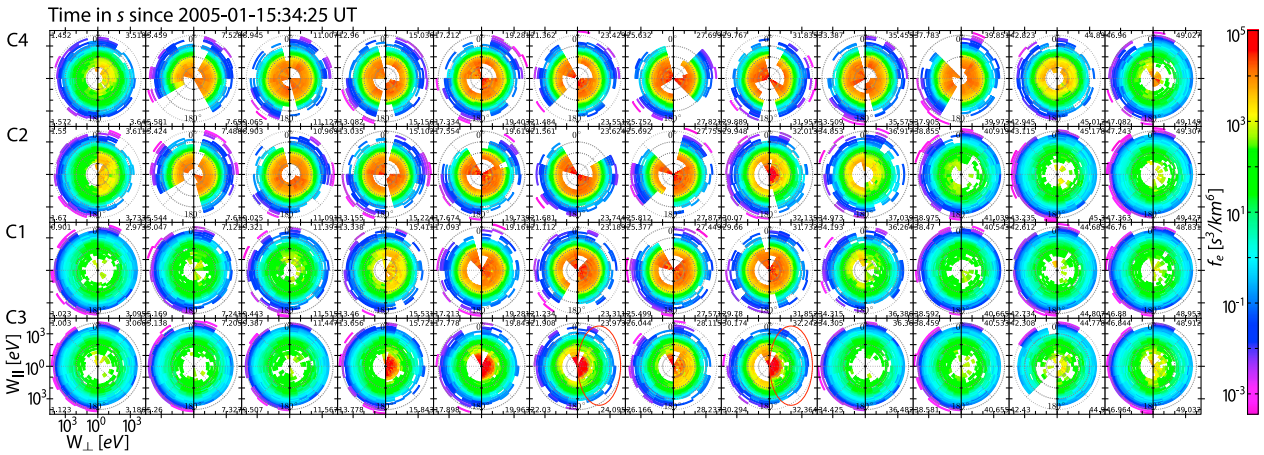


Figure 10. Electron distribution functions during 1534:25–1535:15 UT. Time increases from left to right. The time profiles of the distribution functions are shown in order of increasing spacecraft distance from the magnetopause. For further details, see text.

deeper the closer the spacecraft is to the magnetopause. Further, there are high-frequency magnetic fluctuations in R3, which are absent in R2 and which commence at the R2/R3 boundary.

[24] We suggest that C3 grazes the structure and samples only Region 2, a contention supported in the data so far by the absence of high-frequency magnetic fluctuations.

4.2.2. Electric Field Profiles

[25] Figure 9 shows electric field measurements from the EFW instrument, specifically, the two spin-plane component (X, Y ~GSE) data from the double probe instrument on C4, C1 and C3, plotted at a time resolution of 450 Hz (burst mode). The region boundaries are set by the FGM and CIS data and they clearly order the electric field data well. In particular, strong electric field activity is confined to R2. It does, not, however, extend uniformly throughout the whole R2 region; rather, it occurs in short, discrete bursts, as indicated by arrows in the C3 plot. These fields extend up to ~30 mV/m in both components, at all spacecraft, and last for a fraction of a sec. In the rest of R2 the field is quasistatic.

[26] Figure 9 represents a neat separation of temporal from spatial effects: C3 (most distant from the magnetopause) observes the same activity (localized, intense electric fields) as C1 and C4 do at different times but in the same locale (i.e., R2). It confirms that the strong electric activity in R2 is not a localized feature but occurs at an extended spatial structure. This activity, both quasistatic and bursty, ceases at the R2/R3 boundary.

4.2.3. Electron Distribution Functions in the Vicinity of the Bulge

[27] We now examine electron distribution functions. We give first an overview from the four spacecraft. We then zero in on instances where concurrently episodes of strong electric fields were observed.

[28] In Figure 10 the electron distribution functions measured by all four spacecraft during the bulge (see Figures 8 and 15) traversal 1534:25–1535:15 UT are displayed in time sequence from left to right, and from top to bottom in the same order as in Figure 8 (i.e., C4–C2–C1–C3, in order of increasing distance from the magnetopause). For details about the construction of the distribution array, the reader is referred to *Chen et al.* [2008]. Here we only note that the data are from the PEACE instrument's high-energy sensor (HEEA with an energy range 30 eV to 26 keV), and low-energy sensor (LEEA with an energy range 5 eV to 2.5 keV), e-plotted in log (energy) and pitch angle polar coordinate with 0 degree pitch angle at the top and 180 degree at the bottom of the plot. Each distribution displays data collected in two snapshots as the left-hand and right-hand halves. Each snapshot lasts approximately 1/8 s, and contains data of the same gyrophase from HEEA and LEEA. The two snapshots occur 2 s (half a spacecraft spin) apart. The beginning and end of the data accumulation time (in seconds since 1534:25 UT) are displayed for each snapshot. The distributions have been corrected for photoelectrons, but there may be remnants below 10 eV in some cases or over-correction in others.

[29] The electron distributions inside the main bulge (R3; sketched in Figure 16 below) are indistinguishable from magnetosheath electrons. Consistent with the picture shown in Figure 8, C4 spent the longest time in R3, followed by C2, and then C1. C3 did not detect any magnetosheath electron distributions (did not enter R3 proper), but only grazed the bulge boundary (R2). The first three frames and the last four frames of the distributions measured by C3 are regarded as magnetospheric electrons, while the middle five frames (~1534:38–1534:59 UT) are due to the grazing of R2. The R2 distributions are colder than the magnetospheric distributions but not as dense as the magnetosheath distributions, and they were also detected by C1, C2, and C4. The R2-traversal durations for C1, C2, and C4 are shorter than that for C3, consistent with the grazing interpretation.

[30] A detailed presentation of the electron distributions concurrent with the large-amplitude electric field fluctuations at 1534:49 UT and 1534:58 UT (see red arrows in Figure 9 and red ellipses in Figure 10) is shown in Figure 11. The electrons moving antiparallel to the magnetic field have enhanced phase-space density and extend to higher energies (reaching ~1 keV), consistent with the Hall electron current

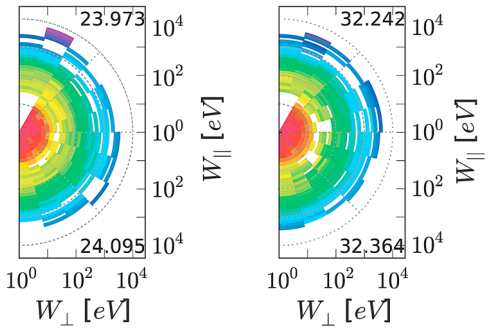


Figure 11. A detailed presentation of the electron distribution concurrent with two large-amplitude electric field fluctuations at 1534:49 UT and 1534:58 UT, corresponding to the times marked by red arrows in Figure 9.

system in the separatrix region [*Asano et al.*, 2008]. We thus interpret the brief intervals with large-amplitude electric field fluctuations in R2 as crossings of the separatrix based on these electron features and that past observations of separatrix crossings at the magnetopause and magnetotail show large-amplitude electric field fluctuations [*André et al.*, 2004; *Khotyaintsev et al.*, 2006; *Chen et al.*, 2009].

[31] Using this interpretation, the spatial scale of the separatrix region may be roughly estimated as follows. The duration of the **E** bursts is of order 0.4 s. Later, in connection with Figure 16, we shall estimate the speed of the bulge with respect to the spacecraft as 110 km s^{-1}. This gives a thickness of ~44 km. With a density near the R2/R3 boundary of ~0.2 cm^{-3} (Figure 15) we have a electron inertial scale, c/ω_{pe}, of ~12 km. So the thickness of the layer is a few c/ω_{pe}. This is consistent with the scale observed

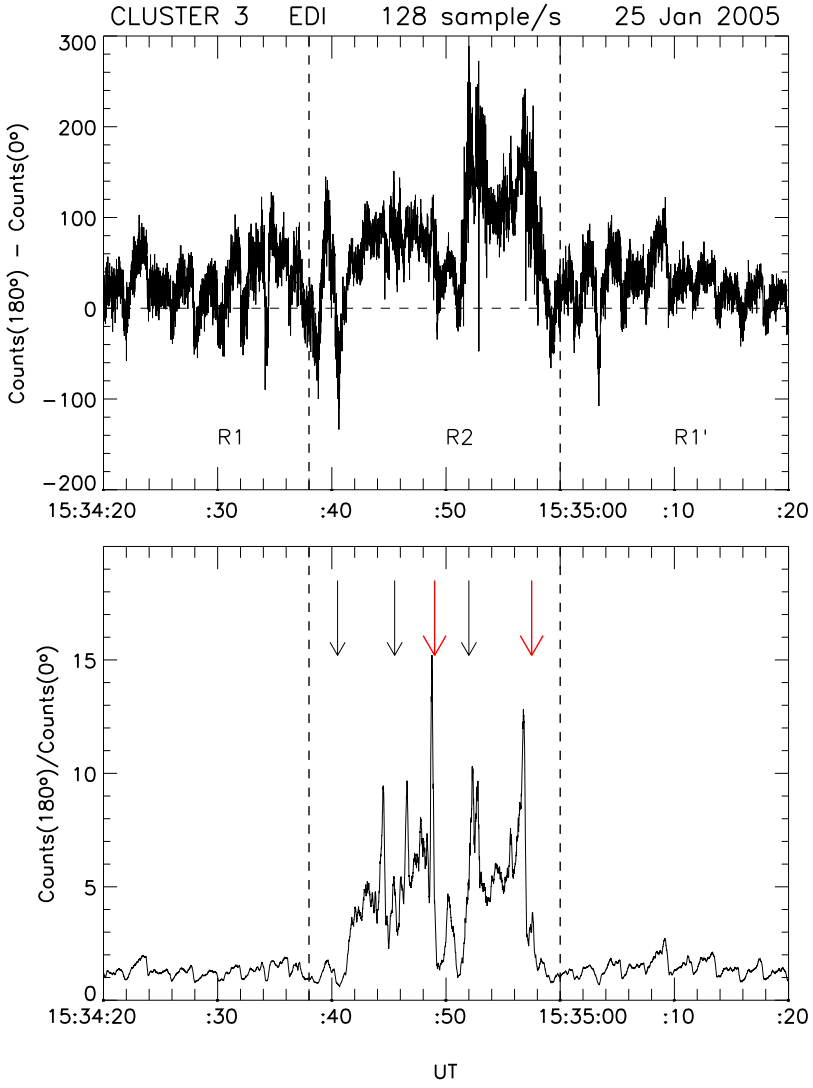


Figure 12. Cluster 3 EDI measurements of fluxes of 500 eV electrons at 128 samples/s resolution. (top) The fluxes antiparallel (180° ± 11.25° pitch angle) less those parallel to the instantaneous field direction. (bottom) The ratio of the 180° to 0° pitch angle fluxes, where a 21 point running average has been formed. The arrow indicates the approximate times of the large-amplitude electric field oscillations shown in Figure 9.

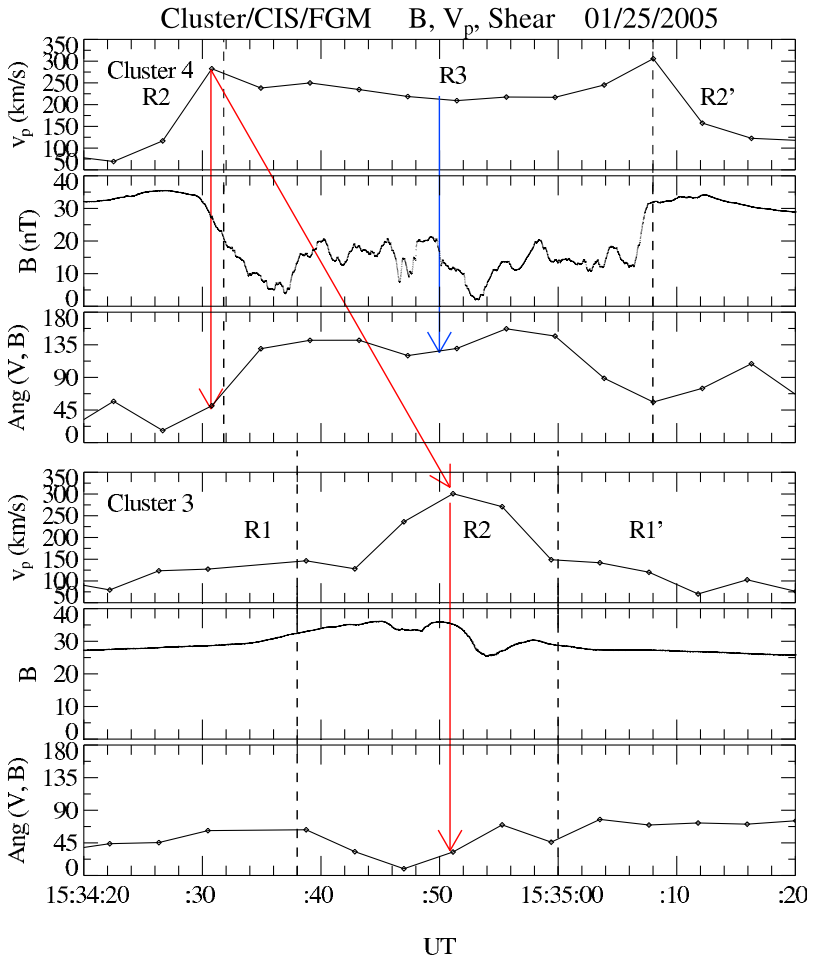


Figure 13. For the interval 1534:20–1535:20 UT, the bulk flow speed, total field strength, and the angle between field and flow vectors are shown from (top) Cluster 4 and (bottom) Cluster 3.

previously [*André et al.*, 2004; *Vaivads et al.*, 2004a, 2004b] and reported from simulations [*Drake et al.*, 2003].

4.2.4. Electron Flows: EDI Observations

[32] We characterize the electron behavior in R2 further by examining observations of 500 eV fluxes at 128 samples/s made by the EDI instrument operating in ambient mode [*Paschmann et al.*, 1997]. (Note that 500 eV electrons are present in this region in the PEACE data above, see Figure 7.) We shall concentrate on C3, which we recall is the spacecraft farthest from the magnetopause and which crosses only R1 and R2. To produce Figure 12 we use a calibration derived on C1 and apply an interdetector efficiency correction to it. Figure 12 (top) shows the difference between the counts of electrons moving antiparallel and those moving parallel to the instantaneous field direction. Figure 12 (bottom) shows the ratio of the 180 to 0° pitch angle counts, where the values have been 21 point smoothed. A clear distinguishing feature of R2 is the bursts of strong flow of 500 eV electrons moving against the field, i.e., toward the X line. This feature is also present in the R2 regions of C1 and C4 (not shown). The times of strongly unbalanced fluxes are in good, though not exact, agreement with the times of electric activity bursts (arrows). This provides further evidence that at these times C3 was crossing a magnetic separatrix.

4.2.5. Plasma Flow Vectors

[33] To illustrate the accelerated plasma flows and their direction with respect to the magnetic field, we consider for simplicity the spacecraft C4 and C3, i.e., the ones closest to, and farthest from, the magnetopause plane, respectively (Figure 4). Figure 13 shows the bulk flow speed, the field strength, and the angle between the field and flow vectors. There are high-speed flows on C4 ("jetting" plasma) in Region R3. However, as for C1 (Figure 6), the highest speeds are attained in R2. The angle the flow makes with the field varies greatly: small in R2 and large in R3, i.e., these angles depend on region. At C4 (and C1, see Figure 6) the flow profile is that of a catenary, with flows peaking in R2 and reaching a relative minimum in R3. At C3, which misses the open field line region R3, the catenary profile is absent and there is just a fast flow which makes a small angle with the magnetic field (red lines in Figure 13 (bottom)). In R2, close to its boundary with R3, we thus have a beam moving approximately parallel to the magnetic field direction. The flow, being along +L, is away from the X line. As the arrows indicate, the beams in region R2 on C4

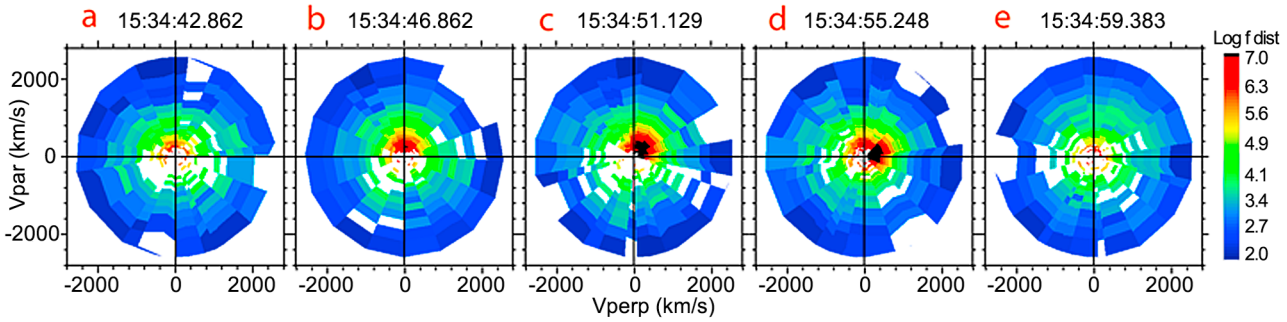


Figure 14. Ion distribution function from C3.

and C3 are of similar speed. They are similar also to values at C1 shown in Figure 6.

[34] In short, there are two kinds of ion plasma jetting in this crater FTEs: (1) fast and approximately field aligned in R2 close to the R2/R3 boundary and (2) slower and subtending a large angle to the magnetic field in R3. As we argue below, the first type of ion plasma are accelerated flows along the separatrices on newly opened field lines, traveling north, away from the X line; the second type of ion plasma are flows in the outflow region ("field reversal" region) on "old" open field lines.

[35] Recall from the section 4.2.4 that there are bursts of electrons moving against the field toward the X line. Together with the high-speed ion beams ("horns" of the catenary profile) in R2 moving along the field away from the X line, we thus have a current in R2, and it is this current which in collisionless reconnection is responsible for the Hall magnetic fields [*Sonnerup*, 1979]. The direction of the ion and electron flows, and their location, provide further strong additional evidence that R2 contains a separatrix which is likely situated near the R2/R3 interface. Its repeated crossing may be due to the fact that the interface is not steady but is subject to fluctuations which makes the separatrix episodically go over the spacecraft.

4.2.6. Ion Distribution Functions

[36] Ion distribution functions from the S3 traversal of the R2 region, from 1534:43 to 1535:00 UT, are shown in Figure 14. These distributions are from the HIA all-ion instrument. They are accumulated over 4 seconds (1 spin) and they cover the 20 eV to 30 keV energy range. The y axis is aligned with the magnetic field while the x axis is perpendicular to the magnetic field direction. The center time of the data accumulation is shown at the top of each distribution.

[37] Although all distributions are acquired from the same region R2 (Figure 14) they show some clear differences. At 1534:47 UT (distribution b) we see an enhancement in the phase space density that indicates the presence of a distinct field-aligned population with a bulk velocity at ~300 km s^{-1}. The timing of this enhancement corresponds to the large amplitude electric field fluctuations shown in Figure 9 and, in particular, to the fluctuations indicated by the second black arrow. The distribution acquired four seconds earlier (distribution a) shows some indication of a field-aligned enhancement but with a smaller bulk velocity. In the next two 4 s intervals (distributions c and d) this population is still present but now it has developed a component perpendicular to the magnetic field too. Four seconds later (distribution e) this distribution is not observed.

4.2.7. Density Profiles

[38] Electron densities, N_e, from WHISPER and ion densities from CIS/HIA or CIS/CODIF (for C4) are shown in Figure 15. From top to bottom we again show the profiles in order of increasing distance from the magnetopause. The regions marked are as defined above. It is seen that in R2 and R2′ the density often decreases to a minimum. This happens close to the interface with R3. There are no indications that this density depression is deeper the closer the spacecraft is to the magnetopause; it seems to be only a property of region (R2) near its boundary with R3. The density decrease near the R2/R3 boundary occurs where the field strength B increases (Figure 8), thus resembling a plasma depletion layer. In fact, kinetic simulations of reconnection just downstream of the separatrices consistently reproduce such a density decrease [*Shay et al.*, 2001; *Ma and Bhattacharjee*, 2001; *Pritchett*, 2001]. It is ascribed to (unmagnetized) ions being expelled perpendicular to the magnetic field by the magnetic pressure.

4.2.8. The Bulge-Shaped Structure of the Reconnection Field Line Region

[39] We may now picture the situation which emerges from the above considerations in the schematic of Figure 16. It shows a projection into the *NL* plane. A bulge of plasma and reconnected field lines constitutes R3. The plasma here is being propelled across the field along the magnetopause in the general L direction by the magnetic tension force. The positions of the four spacecraft earthward of the magnetopause current are shown at a time when C3 is observing an enhanced burst of electric field activity and a flow of electrons toward the X line; that is, it is encountering a separatrix (heavy line). It is also observing an approximately field-aligned proton beam moving away from the X line. At the time shown, the other spacecraft are crossing R3 and they also lie closer to the magnetopause current layer.

[40] We now wish to obtain some idea of the scale sizes of the bulge of reconnected field and plasma passing along the magnetopause from the temporal ordering in the prevailing satellite constellation. We can get the rough geometry as follows. Assume motion in the L direction, as suggested by

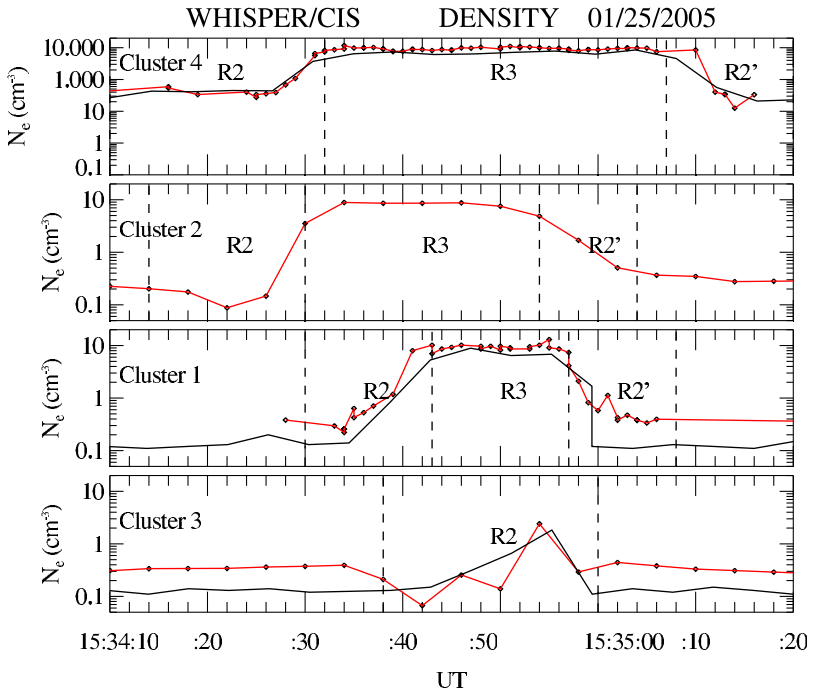


Figure 15. Electron densities from WHISPER (red) and ion densities from CIS/HIA or CIS/CODIF (the latter for C4). The profiles are shown in order of increasing spacecraft distance from the magnetopause.

the fact that C4 and C2 enter the structure (i.e., region R2) at practically the same time. This gives a rough lower limit of the extent of the structure in the M direction of ~1300 km. Consider the motion of the bulge from C4 to C1. The velocity of the structure, V, may be approximated by the arrival of the R2/R3 interface at C4 and, ~10 s later, at C1. With an interspacecraft separation along L of ≈1100 km (Figure 4), we have $V \approx 110$ km s^{-1}. A lower limit to the scale size of the bulge in the L direction is obtained by assuming C4 is exactly at the magnetopause. Using a duration from R1/R2 to R2′/R1's interface passage at C4 of 70 s, this gives $L \approx 7000$ km. During the observations, the Cluster spacecraft stayed on the same side (north) of the X line and on the same side (the magnetosphere side) of the current sheet (magnetopause).

5. Discussion and Conclusions

[41] We have been discussing data on a crater FTEs, paying particular attention to the layer (R2) around the bulge region containing plasma jetting transverse to the reconnected field lines. Previous work, referenced in the Introduction, had shown indications of particle energization there. Using a complement of five instruments and applying the highest time resolution we find that, indeed, there is evidence of energization but it is restricted to an ion-scale layer we identify with a separatrix. The evidence for this consists of (1) short-duration (fraction of a sec) bursts of intense electric field activity (up to ~30 mV/m) and (2) electron beams moving along the field toward the X line at times corresponding roughly to when the bursts of enhanced electric fields are observed. In agreement with previous theoretical and observational work [*Drake et al.*, 2003; *André et al.*, 2004; *Vaivads et al.*, 2004b, 2006; *Khotyaintsev et al.*, 2006; *Asano et al.*, 2008; *Chen et al.*, 2009] we thus identify this few electron scale layer as a separatrix.

[42] This thin layer was shown to be spatially extended and not just a localized feature. Thus, for example, it was seen by all spacecraft in the same region (R2) but at different times. Given the spacecraft configuration and interspacecraft separations in Figure 16, we infer the separatrix to be long, in agreement with conclusions reached in other theoretical and observational work [*Rogers et al.*, 2000;

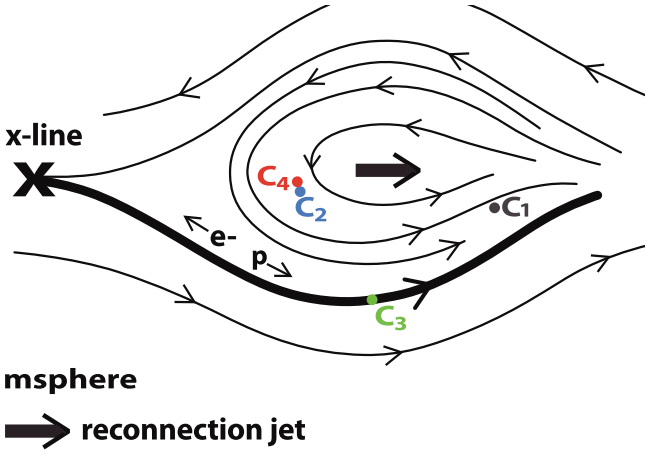


Figure 16. A sketch of the magnetic field configuration at the time when Cluster 3 is observing one of the discrete burst of large-amplitude electric field fluctuations. For further details, see text.

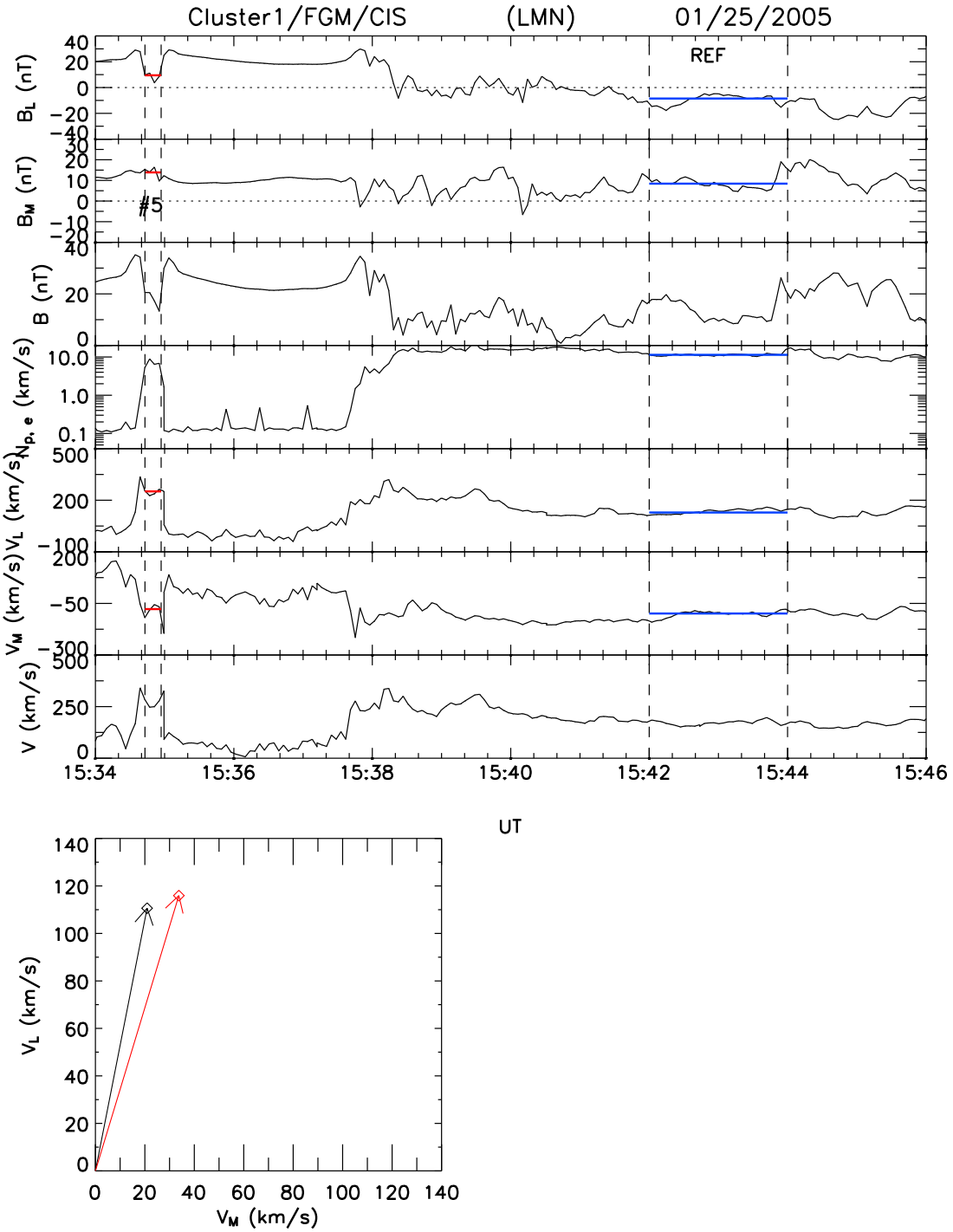


Figure 17. From top to bottom the plots show the L and M components of the magnetic field, the proton density, the L and M component of the flows, and the total flow speed. The vertical dashed lines on the left mark the R3 region of the crater FTE we study. The vertical dashed lines on the right bracket show a 2 min interval of the magnetosheath which is steady and close in time to the observation of the crater FTE we study. The black arrow in the inset shows the average measured velocity in the LM plane, while the red arrow gives that predicted by the Wálen relation.

Shay et al., 2001; *André et al.*, 2004; *Vaivads et al.*, 2004a, 2004b].

[43] We found that the likely place where the separatrix is situated is close to the R2/R3 interface, where there is a maximum in the ion flow speed and a depletion in the density. Separatrices are often identified as boundaries of low-frequency electric field turbulence associated with this density minimum [*Mozer et al.*, 2002], as we also observed.

That the separatrix is repeatedly being crossed may be ascribed to fluctuations of the R2/R3 interface.

[44] While the main focus of this paper is on region R2, we will now briefly discuss R3. Let us look at the jetting plasma there. Is the Walén relation satisfied? We test this on the measurements of C1. Figure 17 shows the relevant quantities: the L and M components of the magnetic field (i.e., in the magnetopause plane), the proton density, the L and M component of the flows and the total flow speed. The vertical dashed lines on the left mark the R3 region of our FTE. The vertical dashed lines on the right bracket a 2 min interval of the magnetosheath which is steady and reasonably close in time to the observation of FTE 5. We work with average quantities and check the average observed changes in V_L and V_M, and the theoretical changes in the same components predicted by the Wálen relation [*Sonnerup et al.*, 1981, equation (7)]. The result is shown in the bottom inset to Figure 17. The black (red) arrows represent the observed (predicted) values of the velocity change. The vectors subtend an angle of 6° to each other and they are of practically equal length. Thus the Wálen relation is satisfied in an average sense. (Figure 17)

[45] Our spacecraft separation in the east-west direction, of order 1000 km, was too small to provide anything but a crude lower limit for the scale size along M (azimuthal). Spacecraft separations of order 10^4 km are required for this. These were attained during the Cluster magnetopause crossing season in 2006. In fact, *Fear et al.* [2008] used Cluster observations at large interspacecraft separation to examine cases of crater FTEs observed on 27 January 2006. They find a poleward size (along the direction of motion, L) varying between 6200–10,300 km. The azimuthal size was estimated from the distant observations to be larger or comparable to the poleward size. The former (L) is in the same range as we derive for our event. As *Fear et al.* [2008] point out, this is consistent with the FTEs being created at a longer X line (or possibly "lines" [*Lee and Fu*, 1985]).

[46] We now mention some literature on reconnection in contexts other than FTEs which have features in common with our observations. In the magnetotail, *Oieroset et al.* [2001] discussed a reversal in the flow jetting direction observed by the Wind spacecraft when it was at 60 R_E downtail just southward of the neutral sheet. Wind started earthward and proceeded to lie tailward of the X line. The fact that the flows reversed without any intervening interval of slow flows lead the authors to suggest that this was an encounter with the (ion) diffusion region. A low-energy (<300 eV) electron beam directed toward the X line was observed at the boundary between the lobe and plasma sheet (i.e., at the "outskirts" of the event). (Electron beams accelerated locally at the separatrix toward the X line were also reported by *Nagai et al.* [2001].) Further, a density decrease was observed which occurred just before the flow reversal. From the latter it was concluded that it was a density dip predicted by models to lie near the separatrices [*Shay et al.*, 2001] rather than in the center of the diffusion region [*Ma and Bhattacharjee*, 2001; *Pritchett*, 2001]. Note that a density cavity near the separatrices was found both in hybrid [*Shay et al.*, 2001] as well as particle-in-cell (PIC) [*Hoshino et al.*, 2001; *Drake et al.*, 2003] simulations.

[47] There are clearly many features in common with our event: the electron beams and their direction, the density cavity, the jetting plasma. The counterpart of the lobe/plasma sheet boundary in our case is the R2/R3 interface. Cluster stayed on one side of the X line and correspondingly saw no flow reversal. Yet, as noted in the Introduction, reversals in the jetting direction were seen in connection with two crater FTEs observed by AMPTE/UKS on 28 September 1984 [see *Farrugia et al.*, 1988, Figure 10]. In these cases the flow did slow down before reversing, giving it had a bifurcated character and implying passage through the inflow region.

[48] In a case study, *Wygant et al.* [2005] studied the structure and dynamics of the reconnection region in the near-tail ($X \approx -18\ R_E$), focussing on the electric field normal to the current sheet (Hall electric field). They used data from a north-to-south crossing of the tail current sheet made by Cluster. During their traversal, the Cluster spacecraft recorded a decrease in the magnetic field strength, which was deepest on that spacecraft crossing the current sheet closest to the X line. Its duration increased with increasing distance from the X line. Our observations are not made during a crossing of the magnetopause current sheet; Cluster stayed earthward of it. So, while Wygant et al. studied signatures moving normal to the current sheet at different distances form the X line, we studied signatures on the same side of the current sheet but also at different distances from the X line. And yet the magnetic field dips are also present, and they are most pronounced at the spacecraft closest to the current sheet (Figure 8).

[49] Topics for future work include (1) a search to see whether "D" distributions of accelerated magnetosheath ions are present. This form of the outflow distribution, exhibiting a cutoff at the Alfvén speed, occurs for acceleration at the magnetopause current sheet due to reconnection and it is considered a direct indication of current sheet acceleration [*Cowley*, 1982, 1994]. (2) Another logical topic is to investigate the ionospheric signatures of crater FTEs.

[50] The moral of the paper is this. One stands to gain by examining crater FTEs. They are numerous enough. (We had six on this pass alone, and a cursory examination of the others show similar features to those reported here.) The microscopic processes leading to macroscopic topology changes and energy conversion may be studied from the encounters with the separatrix embedded in R2, making crater FTEs a veritable "highroad" to the X line. It was indeed a signal breakthrough in reconnection when *Russell and Elphic* [1978] discovered flux transfer events.

[51] **Acknowledgments.** We are very grateful to the referees for their helpful suggestions. Part of this work was done while A.V. was doing summer work at UNH. This work is supported by NASA grants NNX08AD11G and NNG06GD41G and by NASA Cluster grant to UNH.

[52] Masaki Fujimoto thanks the reviewers for their assistance in evaluating this paper.

References

André, M., A. Vaivads, S. C. Buchert, A. N. Fazakerley, and A. Lahiff (2004), Thin electron-scale layers at the magnetopause, *Geophys. Res. Lett.*, *31*, L03803, doi:10.1029/2003GL018137.

Asano, Y., et al. (2008), Electron flat-top distributions around the magnetic reconnection region, *J. Geophys. Res.*, *113*, A01207, doi:10.1029/2007JA012461.

Balogh, A., et al. (1997), The Cluster magnetic field investigation, *Space Sci. Rev.*, *79*, 65–91.

Biernat, H. K., M. F. Heyn, and V. S. Semenov (1987), Unsteady Petschek reconnection, *J. Geophys. Res.*, *92*, 3392–3396.
Chen, L.-J., et al. (2008), Evidence of an extended electron current sheet and its neighboring magnetic island during magnetotail reconnection, *J. Geophys. Res.*, *113*, A12213, doi:10.1029/2008JA013385.
Chen, L.-J., et al. (2009), Multispacecraft observations of the electron current sheet, neighboring magnetic islands, and electron acceleration during magnetotail reconnection, *Phys. Plasmas*, *16*, 056501.
Cowley, S. W. H. (1982), The causes of convection in the Earth's magnetosphere: A review of developments during the IMS, *Rev. Geophys.*, *20*, 531–565.
Cowley, S. W. H. (1994), Earth's plasma environment: Magnetic reconnection and its effect on magnetospheric fields and flows, *Phil. Trans. R. Soc. Lond. A*, *349*, 237–247.
Daly, P. W., and E. Keppler (1983), Remote sensing of a flux transfer event with energetic particles, *J. Geophys. Res.*, *88*, 3971–3980.
Daly, P. W., D. J. Williams, C. T. Russell, and E. Keppler (1981), Particle signature of magnetic flux transfer events at the magnetopause, *J. Geophys. Res.*, *86*, 1628–1632.
Décréau, P. M. E., et al. (2001), Early results from the Whisper instrument on CLUSTER: An overview, *Ann. Geophys.*, *19*, 1241–1258.
Drake, J. F., M. Swisdak, C. Cattell, M. A. Shay, B. N. Rogers, and A. Zeiler (2003), Formation of electron holes and particle energization during magnetic reconnection, *Science*, *299*, 873–977.
Farrugia, C., R. Rijnbeek, M. Saunders, D. Southwood, D. Rodgers, M. Smith, C. Chaloner, D. Hall, P. Christiansen, and L. Woolliscroft (1988), A multi-instrument study of flux transfer event structure, *J. Geophys. Res.*, *93*, 14,465–14,477.
Farrugia, C. J., R. C. Elphic, D. J. Southwood, and S. W. H. Cowley (1987), Field and flow perturbations outside the reconnected field line region in flux transfer events: Theory, *Planet. Space Sci.*, *35*, 227–240.
Fear, R. C., S. E. Milan, A. N. Fazakerley, E. A. Lucek, S. W. H. Cowley, and I. Dandouras (2008), The azimuthal extent of three flux transfer events, *Ann. Geophys.*, *26*, 2353–2369.
Gustafsson, G., et al. (1997), The electric field and wave experiment for the Cluster mission, *Space Sci. Rev.*, *79*, 137–156.
Haerendel, G., G. Paschmann, N. Sckopke, H. Rosenbauer, and P. C. Hedgecock (1978), The frontside boundary layer of the magnetosphere and the problem of reconnection, *J. Geophys. Res.*, *83*, 3195–3216.
Hoshino, M., K. Hiraide, and T. Mukai (2001), Strong electron heating and non-Maxwellian behavior in magnetic reconnection, *Earth Planets Space*, *53*, 627–634.
Johnstone, A. D., et al. (1995), PEACE: A plasma electron and current experiment, *Space Sci. Rev.*, *71*, 351–398.
Khotyaintsev, Y. V., A. Vaivads, A. Retinò, M. André, C. J. Owen, and H. Nilsson (2006), Formation of inner structure of a reconnection separatrix region, *Phys. Rev. Lett.*, *97*, 205003.
LaBelle, J., R. Treumann, G. Haerendel, O. Bauer, G. Paschmann, W. Baumjohann, H. Lühr, R. Anderson, H. Koons, and R. Holzworth (1987), AMPTE IRM observations of waves associated with flux transfer events in the magnetosphere, *J. Geophys. Res.*, *92*, 5827–5843.
Lee, L. C., and Z. F. Fu (1985), A theory of magnetic flux transfer at the Earth's magnetopause, *Geophys. Res. Lett.*, *12*, 105–108.
Lepping, R. P., et al. (1995), The WIND magnetic field investigation, *Space Sci. Rev.*, *71*, 207–229.
Lühr, H., and N. Klöcker (1987), AMPTE-IRM observations of magnetic cavities near the magnetopause, *Geophys. Res. Lett.*, *14*, 186–189.
Ma, Z. W., and A. Bhattacharjee (2001), Hall magnetohydrodynamic reconnection: The Geospace Environment Modeling challenge, *J. Geophys. Res.*, *106*, 3773–3782.
McHenry, M. A., and C. R. Clauer (1987), Modeled ground magnetic signatures of flux transfer events, *J. Geophys. Res.*, *92*, 11,231–11,240.
Moldwin, M., and W. Hughes (1991), Plasmoids as magnetic flux ropes, *J. Geophys. Res.*, *96*, 14,051–14,064.
Mozer, F. S., S. D. Bale, and T. D. Phan (2002), Evidence of diffusion regions at a subsolar magnetopause crossing, *Phys. Rev. Lett.*, *89*, 015001.
Nagai, T., I. Shinohara, M. Fujimoto, M. Hoshino, Y. Saito, S. Machida, and T. Mukai (2001), Geotail observations of the Hall current system: Evidence of magnetic reconnection in the magnetotail, *J. Geophys. Res.*, *106*, 25,929–25,949, doi:10.1029/2001JA900038.
Papamastorakis, I., G. Paschmann, W. Baumjohann, B. U. Ö Sonnerup, and H. Lühr (1989), Orientation, motion, and other properties of flux transfer event structures on September 4, 1984, *J. Geophys. Res.*, *94*, 8852–8866.
Paschmann, G., G. Haerendel, I. Papamastorakis, N. Sckopke, S. J. Bame, J. T. Gosling, and C. T. Russell (1982), Plasma and magnetic field characteristics of magnetic flux transfer events, *J. Geophys. Res.*, *87*, 2159–2168.
Paschmann, G., et al. (1997), The electron drift instrument for Cluster, *Space Sci. Rev.*, *79*, 233–269.
Pritchett, P. L. (2001), Geospace Environment Modeling reconnection challenge: Simulations with a full particle electromagnetic code, *J. Geophys. Res.*, *106*, 3783–3798.
Ogilvie, K. W., et al. (1995), SWE, a comprehensive plasma instrument for the Wind spacecraft, *Space Sci. Rev.*, *71*, 55–77.
Oieroset, M., T. D. Phan, M. Fujimoto, R. P. Lin, and R. P. Lepping (2001), In situ detection of collisionless reconnection in the Earth's magnetotail, *Nature*, *412*, 414–417.
Rème, H., et al. (1997), The CLUSTER Ion Spectrometry Experiment, *Space Sci. Rev.*, *79*, 303–350.
Rijnbeek, R. P., and S. W. H. Cowley (1982), Magnetospheric flux erosion events are flux transfer events, *Nature*, *300*, 135–138.
Rijnbeek, R. P., C. J. Farrugia, D. J. Southwood, M. W. Dunlop, W. A. C. Mier-Jedrzejowicz, C. P. Chaloner, D. S. Hall, and M. F. Smith (1987), A magnetic boundary signature within flux transfer events, *Planet. Space Sci.*, *35*, 871–878.
Rogers, B. N., J. F. Drake, and M. A. Shay (2000), The onset of turbulence in collisionless magnetic reconnection, *Geophys. Res. Lett.*, *27*, 3157–3160.
Russell, C. T., and R. C. Elphic (1978), Initial ISEE magnetometer results: Magnetopause observations, *Space Sci. Rev.*, *22*, 681–715.
Saunders, M. A., C. T. Russell, and N. Sckopke (1984), Flux transfer events: Scale size and internal structure, *Geophys. Res. Lett.*, *11*, 131–134.
Scholer, M. (1988), Magnetic flux transfer at the magnetopause based on single X line bursty reconnection, *Geophys. Res. Lett.*, *15*, 291–294.
Scholer, M., D. Hovestadt, F. Ipavich, and G. Gloeckler (1982), Energetic protons, alpha particles, and electrons in magnetic flux transfer events, *J. Geophys. Res.*, *87*, 2169–2175.
Scudder, J. D., K. W. Ogilvie, and C. T. Russell (1984), The relation of flux transfer events to magnetic reconnection, in *Magnetic Reconnection in Space and Laboratory Plasmas*, edited by E. W. Hones Jr., p. 151, AGU, Washington, D. C.
Shay, M. A., J. F. Drake, B. N. Rogers, and R. E. Denton (2001), Alfvénic collisionless magnetic reconnection and the Hall term, *J. Geophys. Res.*, *106*, 3759–3772.
Slavin, J. A., et al. (1989), CDAW 8 observations of plasmoid signatures in the geomagnetic tail: An assessment, *J. Geophys. Res.*, *94*, 15,153–15,175.
Sonnerup, B. U. Ö. (1979), *Solar System Plasma Physics*, vol. 3, edited by L. T. Lanzerotti, C. F. Kennel, and E. N. Parker, pp. 45–108, North-Holland, New York.
Sonnerup, B. U. Ö. (1987), On the stress balance in flux transfer events, *J. Geophys. Res.*, *92*, 8613–8629.
Sonnerup, B. U. Ö., G. Paschmann, I. Papamastorakis, N. Sckopke, G. Haerendel, S. Bame, J. Asbridge, J. Gosling, and C. Russell (1981), Evidence for Magnetic Field Reconnection at the Earth's Magnetopause, *J. Geophys. Res.*, *86*, 10,049–10,067.
Southwood, D. J. (1985), Theoretical aspects of ionosphere-magnetosphere-solar wind coupling, *Adv. Space Res.*, *5*, 7–14, doi:10.1016/0273-1177(85)90110-3.
Southwood, D. J. (1987), The ionopsheric signature of flux transfer events, *J. Geophys. Res.*, *92*, 3207–3213.
Southwood, D. J., C. J. Farrugia, and M. A. Saunders (1988), What are flux transfer events?, *Planet. Space Sci.*, *36*, 503–508.
Vaivads, A., M. André, S. C. Burchert, J.-E. Wahlund, A. N. Fazakerley, and N. Cornilleau-Wehrlin (2004a), Cluster observations of lower hybrid turbulence within thin layers at the magnetopause, *Geophys. Res. Lett.*, *31*, L03804, doi:10.1029/2003GL018142.
Vaivads, A., Y. Khotyaintsev, M. André, A. Retinò, S. C. Buchert, B. N. Rogers, P. Décréau, G. Paschmann, and T. D. Phan (2004b), Structure of the magnetic reconnection diffusion region from four-spacecraft observations, *Phys. Rev. Lett.*, *93*, 105001.
Vaivads, A., A. Retinò, and M. Andrè (2006), Microphysics of magnetic reconnection, *Space Sci. Rev.*, *122*, 19–27.
Walthour, D., B. U. Ö. Sonnerup, G. Paschmann, H. Lühr, D. Klumpar, and T. Potemra (1993), Remote sensing of two-dimensional magnetopause structures, *J. Geophys. Res.*, *98*, 1489–1504.
Wygant, J. R., et al. (2005), Cluster observations of an intense normal component of the electric field at a thin reconnecting current sheet in the tail and its role in the shock-like acceleration of the ion fluid into the separatrix region, *J. Geophys. Res.*, *110*, A09206, doi:10.1029/2004JA010708.

M. André and A. Vaivads, Swedish Institute of Space Physics, Box 537, SE-751 21 Uppsala, Sweden.

L.-J. Chen, C. J. Farrugia, C. Mouikis, C. W. Smith, R. B. Torbert, and H. Vaith, Space Science Center, Department of Physics, University of New Hampshire, 39 College Rd., Morse Hall, Rm. 414, Durham, NH 03824, USA. (charlie.farrugia@unh.edu)

S. W. H. Cowley, Department of Physics and Astronomy, University of Leicester, University Road, Leicester LE1 7RH, UK.

P. Décréau, LPCE2/CNRS, 3A av. de la Recherche Scientifique, Orleans F-45071, France.

E. Lucek, Space and Atmospheric Physics Group, Imperial College of Science and Technology, London SW7 2BW, UK.

C. J. Owen, Mullard Space Science Laboratory, University College London, London RH5 6NT, UK.

D. J. Sibeck, NASA Goddard Space Flight Center, Code 674, 8800 Greenbelt Rd., Greenbelt, MD 20771, USA.

D. J. Southwood, European Space Agency Headquarters, Paris F-75738, France.

A. Vrublevskis, Plasma Science and Fusion Center, Massachusetts Institute of Technology, Cambridge, MA 02142, USA.